PFC/RR-90-2 DOE/ET-51013-279

TSC Simulations of Alcator C-MOD Discharges II: Single X-Point, Vertically Asymmetric Scenario

J.J. Ramos

Plasma Fusion Center
Massachusetts Institute of Technology
Cambridge, MA 02139

January 1990

This work was supported by the U. S. Department of Energy Contract No. DE-AC02-78ET51013. Reproduction, translation, publication, use and disposal, in whole or in part by or for the United States government is permitted.

TSC Simulations of Alcator C-MOD Discharges
II: Single X-Point, Vertically Asymmetric Scenario

J. J. Ramos
PLASMA FUSION CENTER, MIT, Cambridge, MA 02139

Abstract

A simulation of a single X-point diverted discharge of the Alcator C-MOD tokamak is carried out using the Tokamak Simulation Code (TSC).

In a previous report [1], we presented a dynamical simulation of the Alcator C-MOD tokamak, carried out with the Tokamak Simulation Code (TSC) [2], under the assumption of perfect vertical symmetry. The actual Alcator C-MOD device will have a single X-point divertor and, therefore, will lack vertical symmetry. The purpose of the present report is to investigate the realistic single X-point scenario.

Some modifications in the computational model have been introduced relative to the one used in Ref. 1. The computational domain has been enlarged slightly to a 0.90 m by 1.48 m rectangle with grid points 0.02 m apart. A more complete and realistic model of the vacuum vessel has been introduced as illustrated in Fig. 1. The upper and lower sections of the OH2 and EF1 coils are now independent of each other. Finally, the vertical control coil EFC, with its upper and lower sections connected in antiseries to a single power supply, has been incorporated. In total, there are 8 independent coil groups plus the vacuum vessel within the computational domain. Their characteristics are given in the following table.

Table I:

COIL	NO. OF FILAMENTS IN OUR MODEL	ACTUAL NO. OF TURNS
OH1 (nose plus upper and lower ears)	76	130
OH2U (upper)	18	27
OH2L (lower)	18	27
EF1U (upper)	25	94
EF1L (lower)	25	94
EF2 (upper plus lower)	50	194
EF3 (upper plus lower)	56	150
EFC (upper and lower connected in antiseries)	8	36
Vacuum Vessel	285	

The EF4 coil, with its upper and lower sections in series, is outside the computational grid and is modeled as a single filament located at its geometrical center.

Like in Ref. 1, we simulate a 3s long discharge with a 1s current rise phase, a 1s flat-top with 3Mamp of plasma current, and a 1s ramp-down. The vacuum toroidal field is increased linearly from 6T to 9T at R=0.665m during the current ramp-up, is held constant at 9T through the flat-top, and is brought back to 6T during the current ramp-down. Figures 2 and 3 show the time dependence of the plasma current and the toroidal field. The plasma current is induced by appropriate variation of the poloidal flux and the plasma temperature increases as the result of ohmic heating. No current drive or auxiliary heating are included in the present simulation. The plasma fueling is simulated by a prescribed time dependence of the particle density which is shown in Fig. 4.

A full-size, diverted configuration is reached at t=0.2s when the plasma current equals 1.2Mamp. Thereafter, the geometry of the plasma boundary and the location of the X-point remain virtually constant for the remainder of the ramp-up phase and until the end of the flat-top. Figures 5 through 8 display the toroidal current density and the poloidal flux at different stages of the discharge: t=0, I=50Kamp corresponds to the beginning of our simulation, shortly after the plasma breakdown; t=0.14s, I=0.67Mamp corresponds to a limiter-bound state before the separatrix is formed; at t=0.40s, I=1.94Mamp the plasma has its final geometrical shape; finally at t=1.50s, I=3.00Mamp we have a full current state at the middle of the flat-top. The time dependence of the major radius, minor radius, elongation, triangularity and X-point coordinates is shown in Figures 9 through 14. In its quiescent phase, the plasma major radius equals 0.665m, the minor radius is equal to 0.21m, the separatrix elongation and triangularity are $\kappa_x = 1.75$, $\delta_x = 0.4$, and at

the 95% relative to the separatrix flux surface $\kappa_{95} = 1.6$, $\delta_{95} = 0.3$. Figure 15 summarizes the evolution of the plasma shape from start-up through the middle of flat-top, whereas Fig. 16 does so from the middle of flat-top until the end of the ramp-down.

Five independent active feedback systems are used to control the plasma position and shape as well as its induced current. The first one acts on coil EF3 and controls the radial position of the plasma. The second and third ones act on quadruple field producing combinations of OH2U, EF1U and EF2, and OH2L, EF1L and EF2, respectively, and control the upper and lower elongation of the plasma. The fourth one acts on a combination of OH1, OH2U, OH2L, EF1U, EF1L, EF2 and EF3, that produces an approximate field null and is used to control the evolution of the plasma current. The fifth one acts on the EFC coil and controls the vertical position of the plasma. The issue of vertical control and axisymmetric stability will be studied thoroughly in a forthcoming report. The external EF4 coil is not part of any feedback system since the thick metal structure that exists between it and the plasma should result in a slow field penetration.

Figures 17 through 20 show the safety factor, the plasma beta, the peak temperatures and the confinement time as functions of time. The poloidal flux consumption is illustrated in Fig. 21. The flux swings from -2.39 volt-s at the beginning of our simulation to a maximum of +4.45 volt-s at the end of the flat-top. In calculating the plasma resistivity, Z_{eff} was set equal to 1.5 throughout the discharge.

The time histories of the PF coil currents are plotted in Figs. 22 through 30, along with the corresponding voltages. Quantities plotted correspond to one filament of our model, so that use of Table I should be made to calculate the corresponding values per actual turn or for the whole coil. Figure 31 shows the induced currents in the vacuum

vessel. Several constraints aimed at optimizing the use of power supplies and discussed in Ref. 1 are satisfied, but we must allow for a sign change in the currents of the EF1 coils during the discharge. The current in EF4 is the preprogrammed one as this coil does not belong to any feedback system. Conversely, EFC has no preprogrammed current, and Fig. 30 shows only the result of the active vertical control system. However, this output does not represent the actual requirement for vertical control because in the present simulation, the growth rate of the ideal MHD axisymmetric instability has been artificially reduced by largely enhancing the ion mass. This is done in order to reduce the disparity between the Alfven and transport time scales, and therefore be able to account for both types of phenomena in the numerical simulation of a long lived, 3s tokamak discharge. The proper treatment of the axisymmetric instability and its active control will be thoroughly dealt with in a separate report.

Acknowledgements

The author thanks S. Jardin for providing the TSC code and offering continuous assistance in its running. He also appreciates the useful discussions and help provided by the members of the Alcator group, especially S. Fairfax, P. Hakkarainen, I. Hutchinson and S. Wolfe. This work was supported by the U.S. Department of Energy under contract No. DE-AC02-78ET51013.

References

[1] J.J. Ramos, M.I.T. Report PFC/RR-88-9 (1988).

[2] S.C. Jardin, N. Pomphrey, and J. DeLucia, J. Computational Phys. 66, 481 (1986).

Figure Captions

Fig. 1 Computational grid and model and vacuum vessel and PF coils.

Fig. 2 Plasma current versus time.

Fig. 3 Toroidal field stream function $(RB_t)_{vacuum}$ versus time.

Fig. 4 Particle density versus time. The three traces show the central, line average and volume average values.

Fig. 5 Toroidal current density and poloidal flux at initiation, t=0.

Fig. 6 Toroidal current density and poloidal flux at t=0.14s.

Fig. 7 Toroidal current density and poloidal flux at t=0.40s.

Fig. 8 Toroidal current density and poloidal flux at the middle of flat-top, t=1.50s.

Fig. 9 Major radius versus time.

Fig. 10 Minor radius versus time.

Fig. 11 Plasma elongation versus time. The different traces correspond to 90%, 95% and edge flux surfaces. The latter is defined by either the limiter or the separatrix flux surface.

Fig. 12 Plasma triangularity in terms of the 90%, 95% and edge flux surfaces, versus time.

Fig. 13 Radial position of the separatrix X-point versus time, shown for the time interval where the separatrix defines the plasma edge.

Fig. 14 Axial position of the separatrix X-point versus time.

Fig. 15 Evolution of the plasma edge from start-up to the middle of flat-top.

Fig. 16 Evolution of the plasma edge from the middle of flat-top to the end of ramp-down.

Fig. 17 Safety factor q versus time. The different traces correspond to the 99.9% and 95% flux surfaces, the cylindrical q and the elongation corrected cylindrical q_*.

Fig. 18 Plasma beta versus time. The different traces show half the central value and the average values in terms of the volume averaged field and the vacuum field at the center, respectively.

Fig. 19 Peak electron and ion temperatures in eV versus time.

Fig. 20 Energy confinement time versus time.

Fig. 21 Poloidal flux versus time.

Fig. 22 Current and voltage in OH1 coil versus time. Magnitudes plotted correspond to one filament of our model.

Fig. 23 Current and voltage in OH2U coil.

Fig. 24 Current and voltage in OH2L coil.

Fig. 25 Current and voltage in EF1U coil.

Fig. 26 Current and voltage in EF1L coil.

Fig. 27 Current and voltage in EF2 coil.

Fig. 28 Current and voltage in EF3 coil.

Fig. 29 Current and voltage in EF4 coil.

Fig. 30 Current in EFC coil.

Fig. 31 Induced currents in vacuum vessel versus time.

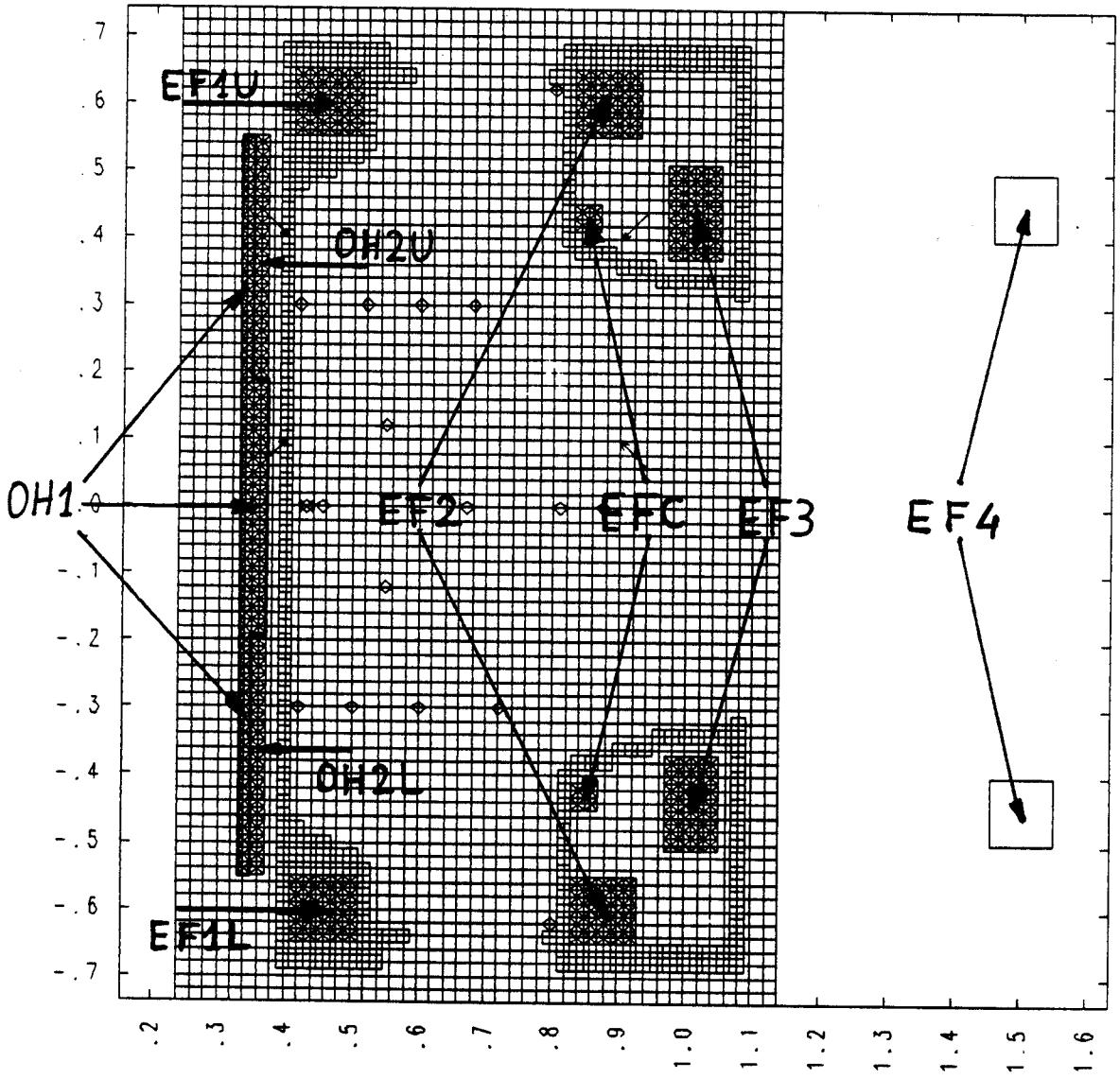
EF4U
OH2U
OH1
EF2
EFC
EF3
EF4
OH2L
EF1L
.7
.6
.5
.4
.3
.2
.1
0
-.1
-.2
-.3
-.4
-.5
-.6
-.7
.2
.3
.4
.5
.6
.7
.8
.9
1.0
1.1
1.2
1.3
1.4
1.5
1.6

Figure 1

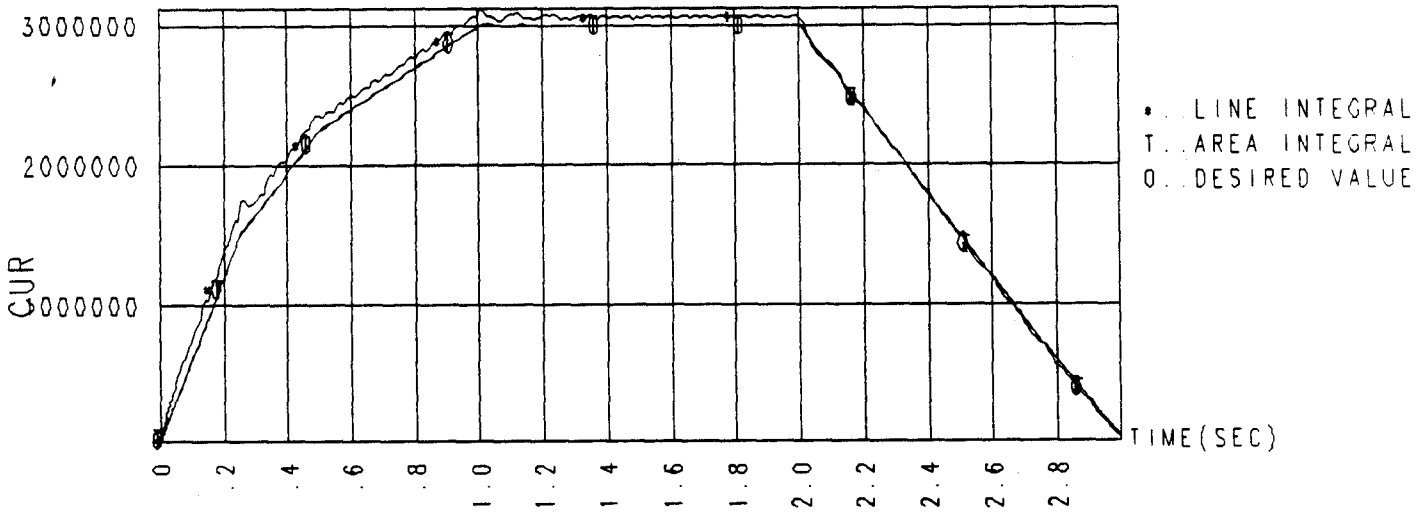
3000000
2000000
CUR
0000000
. LINE INTEGRAL
T. AREA INTEGRAL
O. DESIRED VALUE
TIME(SEC)
0
.2
.4
.6
.8
1.0
1.2
1.4
1.6
1.8
2.0
2.2
2.4
2.6
2.8

Figure 2

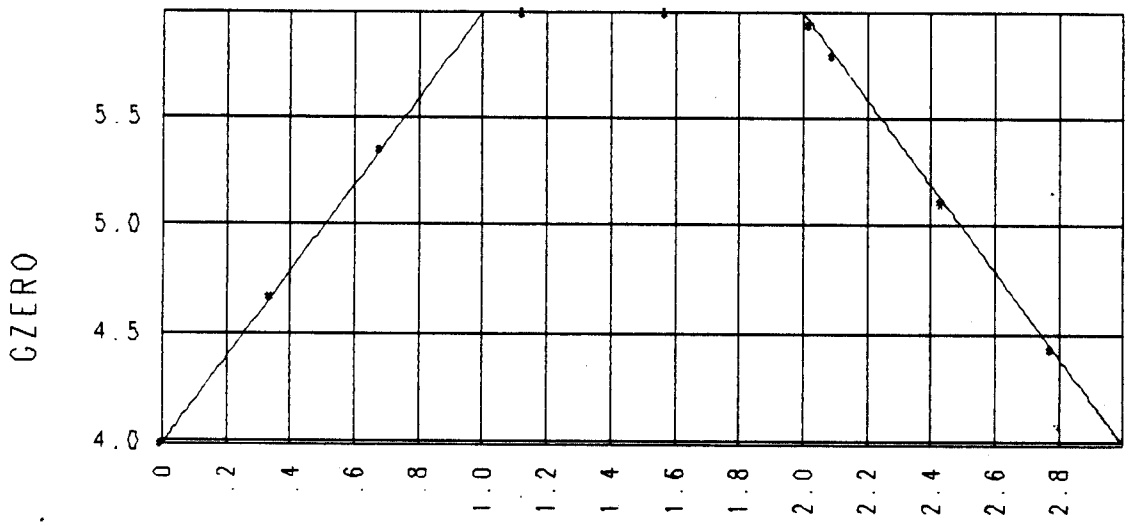

Figure 3

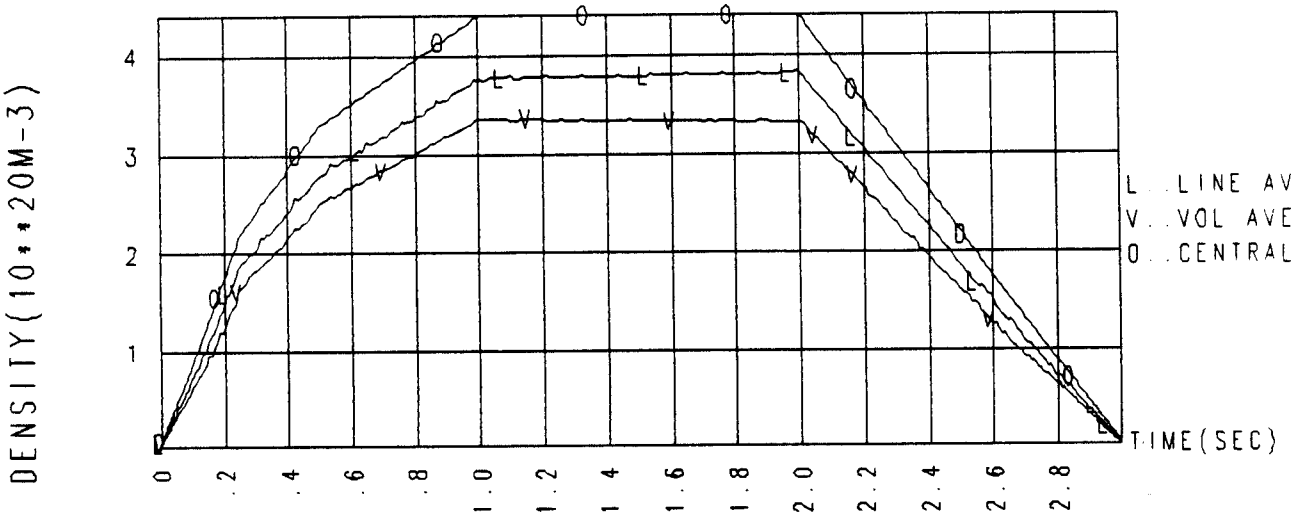
DENSITY(10**20M-3)
4
3
2
1
0
.2
.4
.6
.8
1.0
1.2
1.4
1.6
1.8
2.0
2.2
2.4
2.6
2.8
TIME(SEC)
L..LINE AV
V..VOL AVE
O..CENTRAL

Figure 4

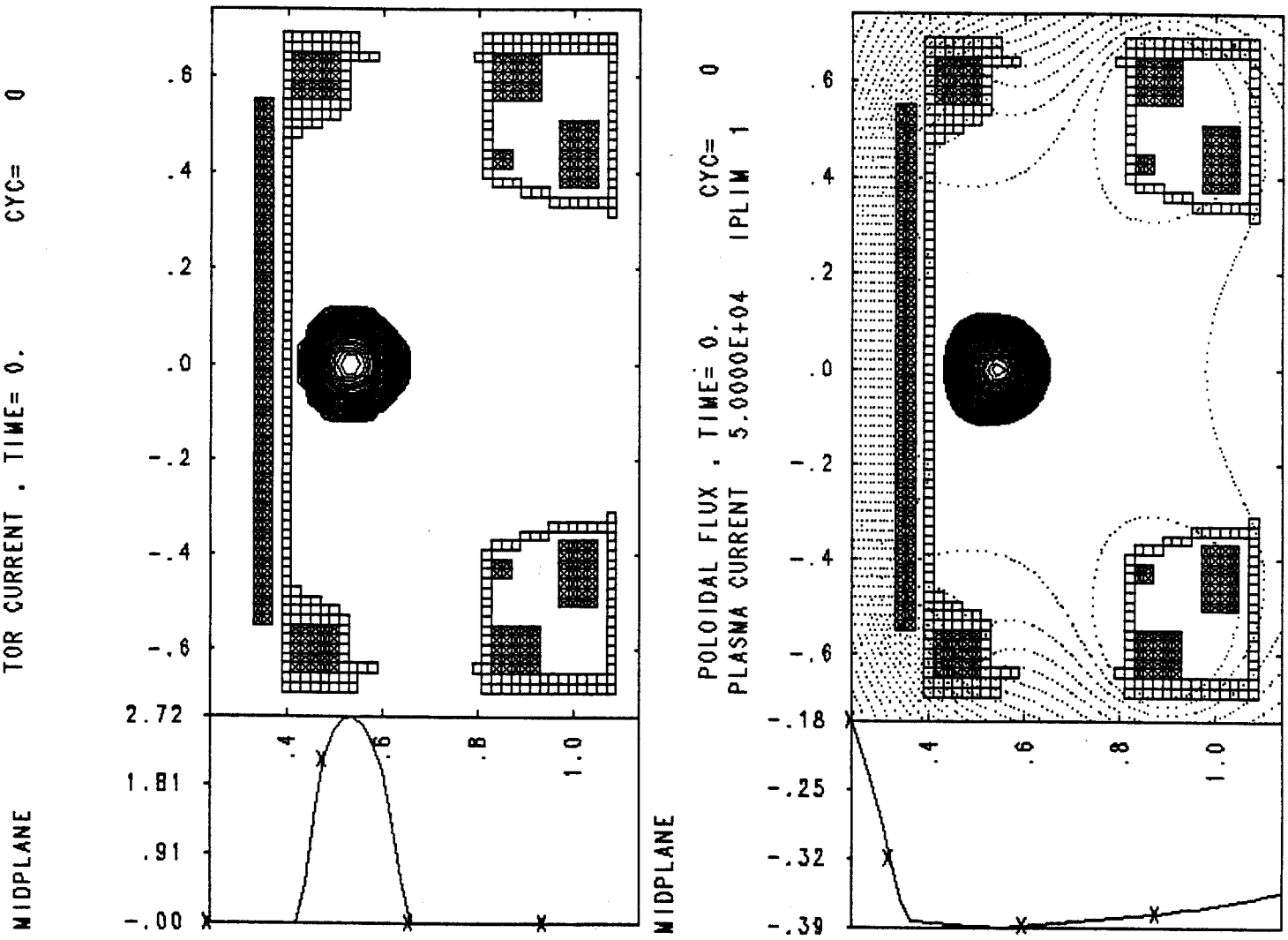
TOR CURRENT . TIME= 0. CYC= 0
.6
.4
.2
.0
-.2
-.4
-.6
2.72
1.81
.91
-.00
.4
.6
.8
1.0
MIDPLANE
MIDPLANE
POLOIDAL FLUX . TIME= 0. CYC= 0
PLASMA CURRENT 5.0000E+04 IPLIM 1
.6
.4
.2
.0
-.2
-.4
-.6
-.18
-.25
-.32
-.39
.4
.6
.8
1.0

Figure 5

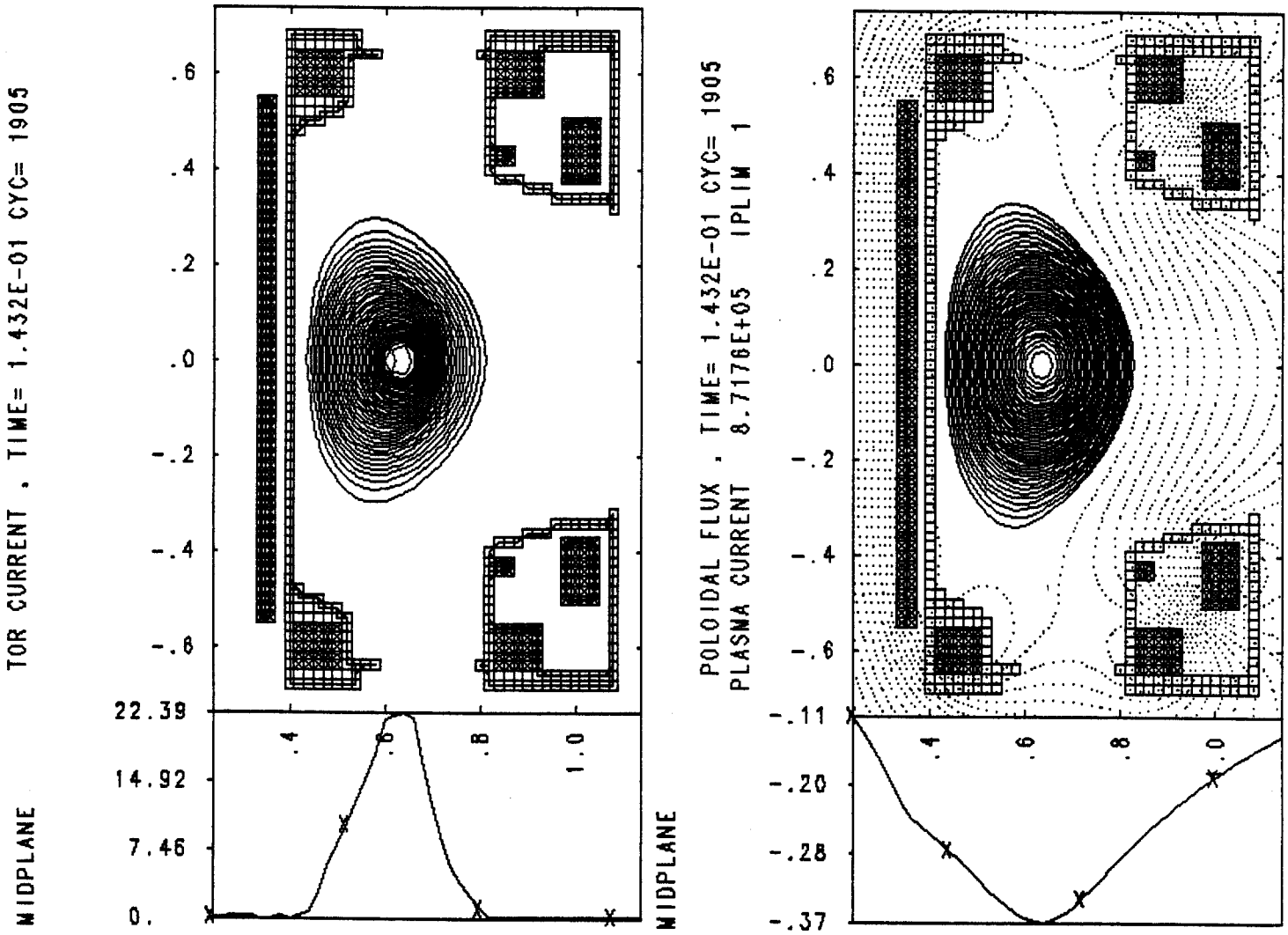
TOR CURRENT . TIME= 1.432E-01 CYC= 1905
.6
.4
.2
.0
-.2
-.4
-.6
22.39
14.92
7.46
0.
.4
.6
.8
1.0
MIDPLANE
POLOIDAL FLUX . TIME= 1.432E-01 CYC= 1905
PLASMA CURRENT = 8.7176E+05 IPLIM 1
.6
.4
.2
.0
-.2
-.4
-.6
-.11
-.20
-.28
-.37
.4
.6
.8
.0
MIDPLANE

Figure 6

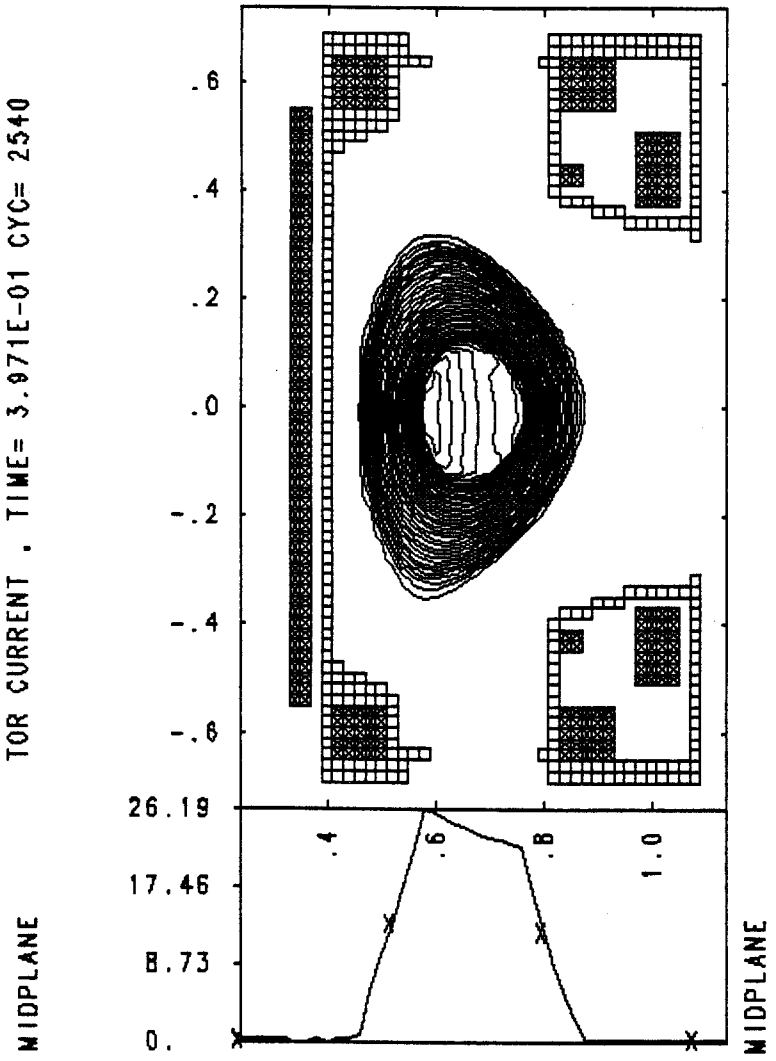
TOR CURRENT . TIME= 3.971E-01 CYC= 2540
.6
.4
.2
.0
-.2
-.4
-.6
26.19
17.46
8.73
0.
.4
.6
.8
1.0
MIDPLANE
MIDPLANE

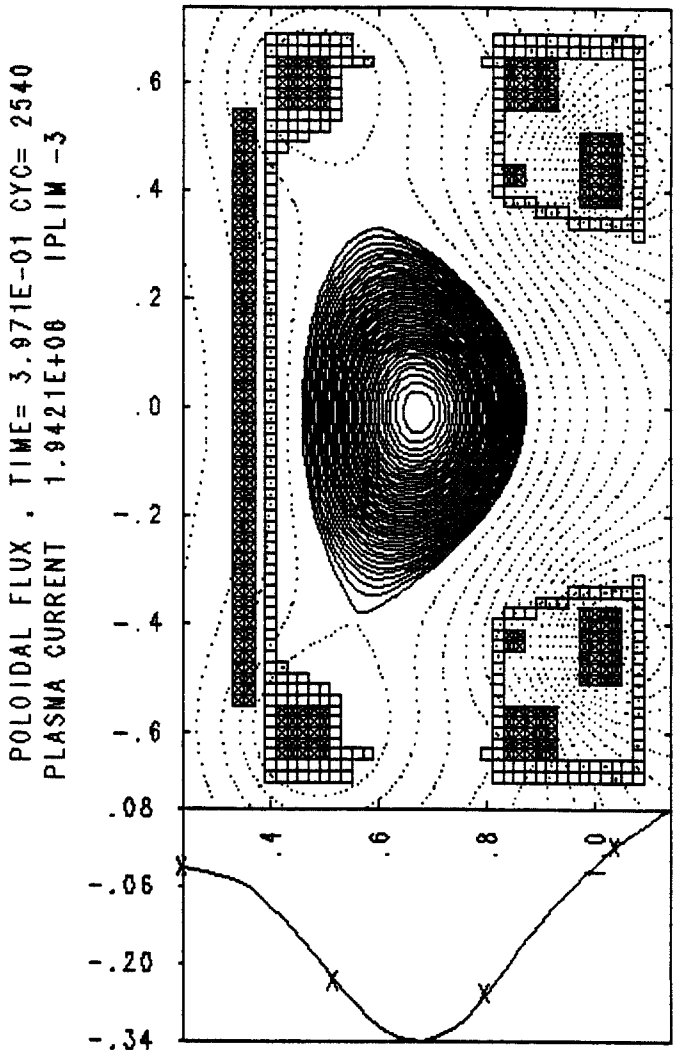
POLOIDAL FLUX . TIME= 3.971E-01 CYC= 2540
PLASMA CURRENT 1.9421E+06 IPLIM -3
.6
.4
.2
.0
-.2
-.4
-.6
.08
-.06
-.20
-.34
.4
.6
.8
1.0

Figure 7

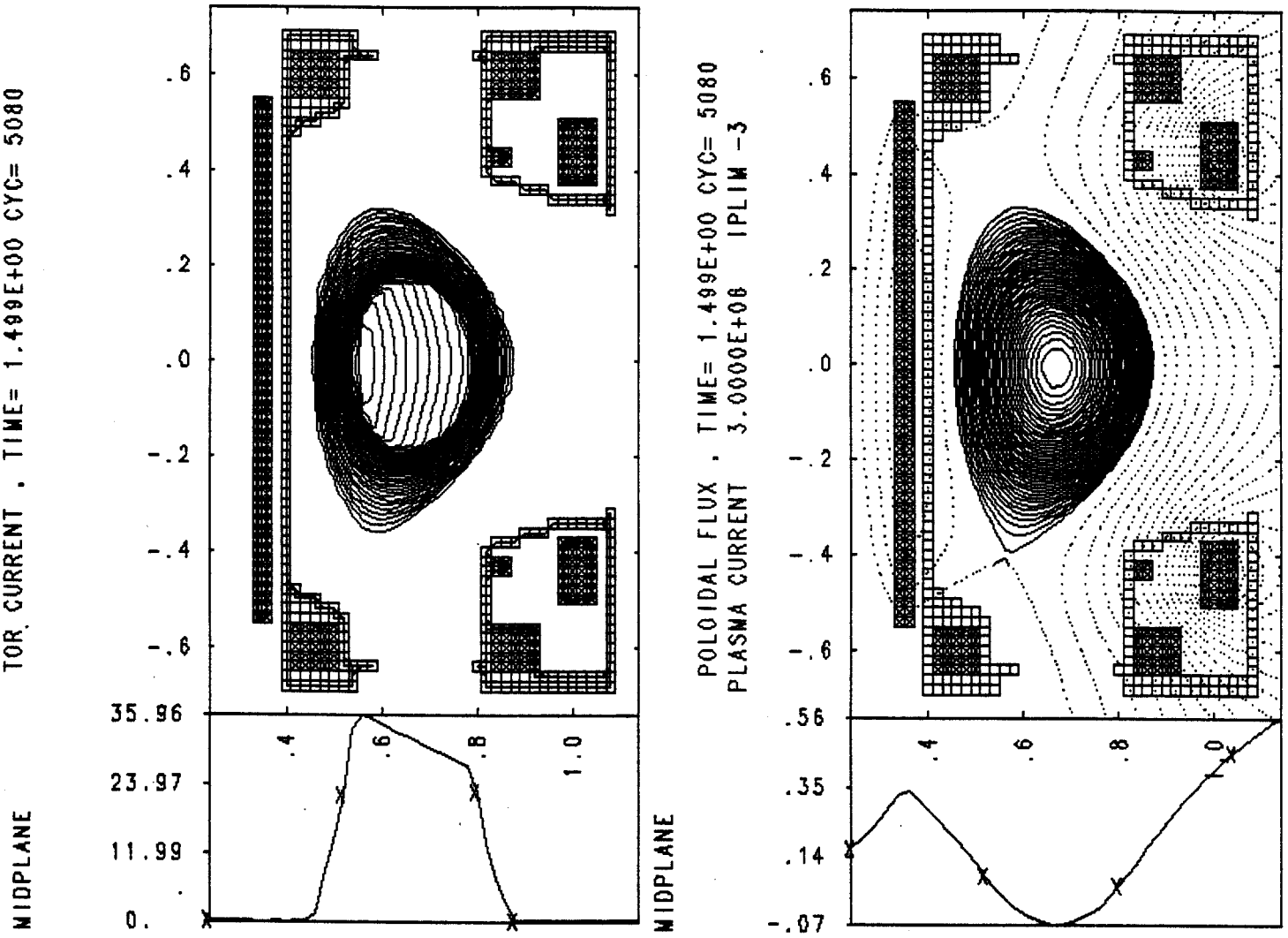
TOR. CURRENT . TIME= 1.499E+00 CYC= 5080
.6
.4
.2
.0
-.2
-.4
-.6
35.96
23.97
11.99
0.
.4
.6
.8
1.0
MIDPLANE
POLOIDAL FLUX . TIME= 1.499E+00 CYC= 5080
PLASMA CURRENT 3.0000E+06 IPLIM -3
.6
.4
.2
.0
-.2
-.4
-.6
.56
.35
.14
-.07
.4
.6
.8
.0
MIDPLANE

Figure 8

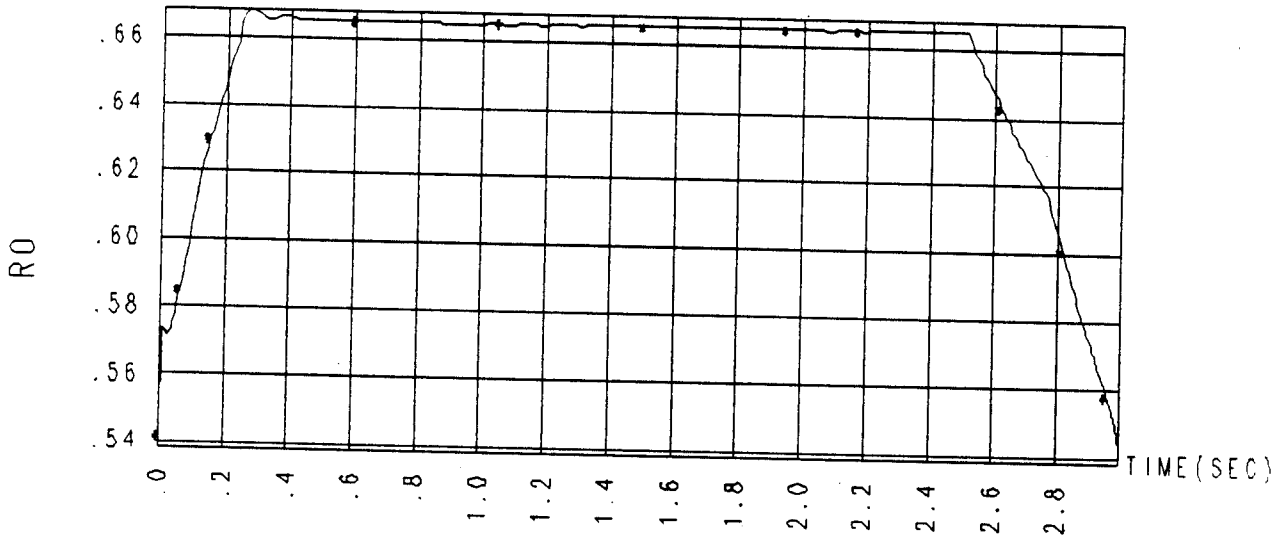

Figure 9

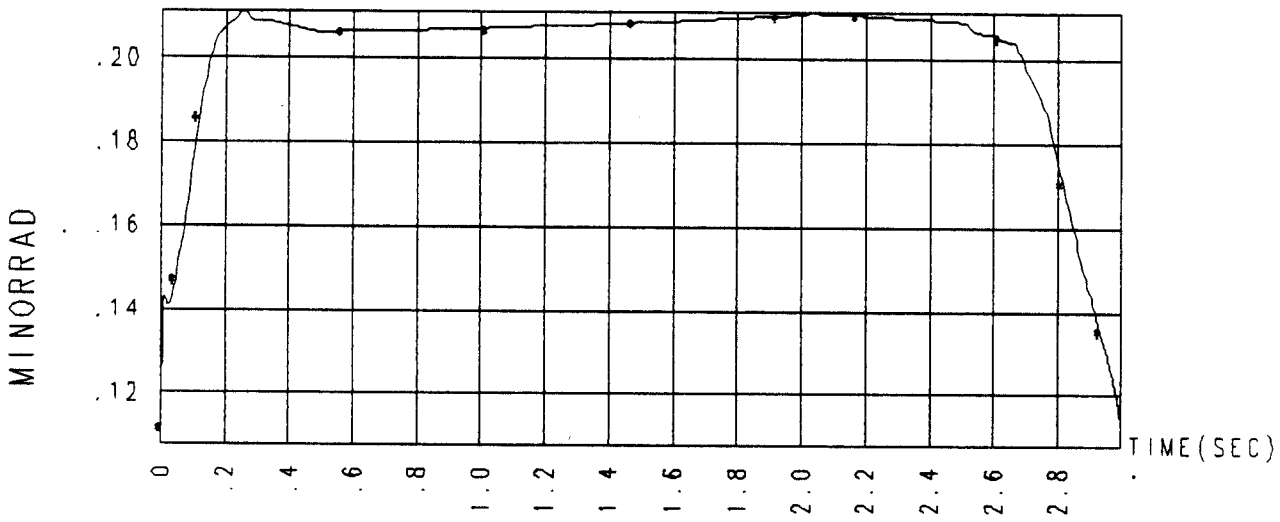
MINORRAD
.20
.18
.16
.14
.12
0
.2
.4
.6
.8
1.0
1.2
1.4
1.6
1.8
2.0
2.2
2.4
2.6
2.8
TIME(SEC)

Figure 10

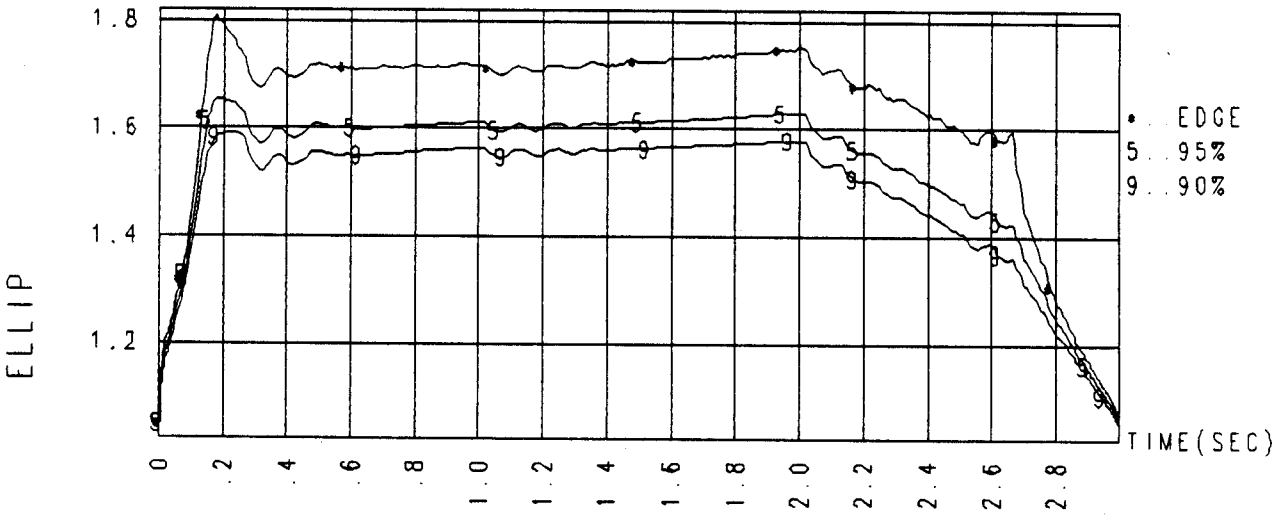
ELLIP
1.8
1.6
1.4
1.2
0
.2
.4
.6
.8
1.0
1.2
1.4
1.6
1.8
2.0
2.2
2.4
2.6
2.8
TIME(SEC)
. EDGE
5 . 95%
9 . 90%

Figure 11

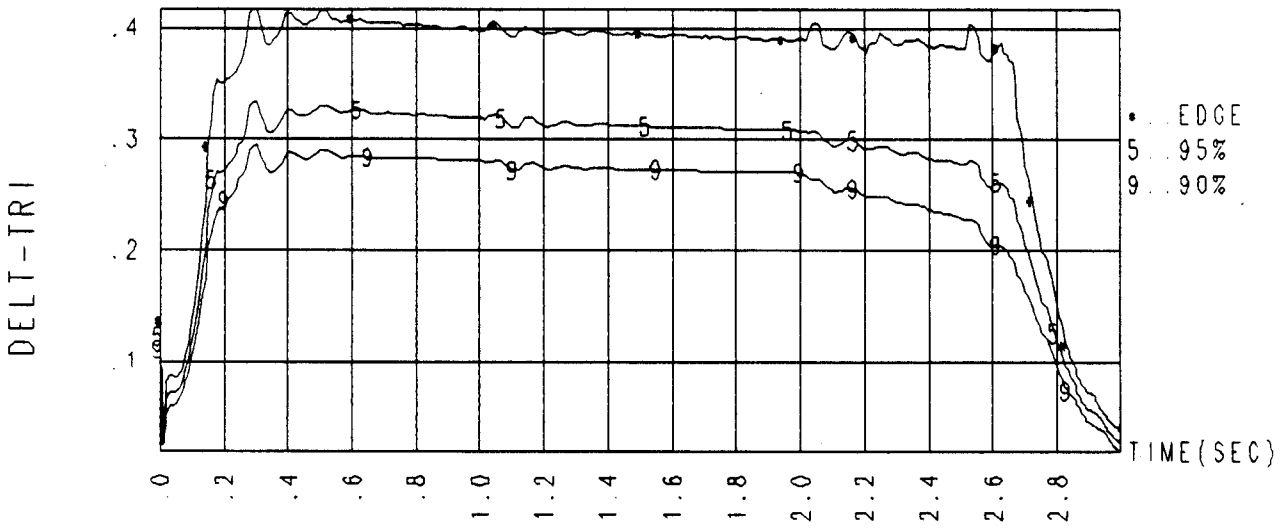
DELT-TRI
.4
.3
.2
.1
0
.2
.4
.6
.8
1.0
1.2
1.4
1.6
1.8
2.0
2.2
2.4
2.6
2.8
TIME(SEC)
EDGE
95%
90%

Figure 12

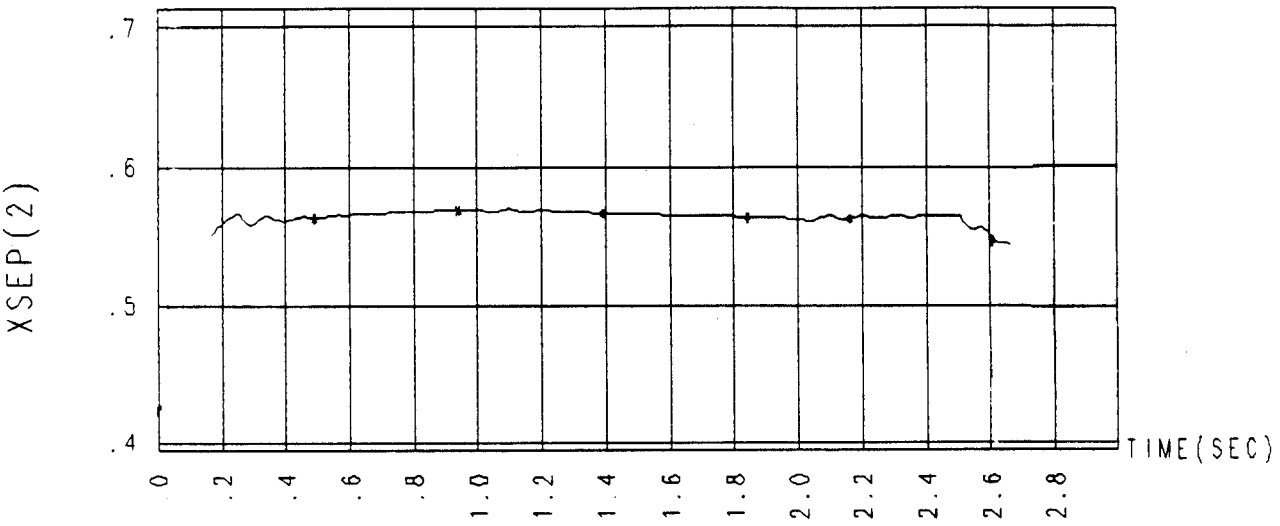

Figure 13

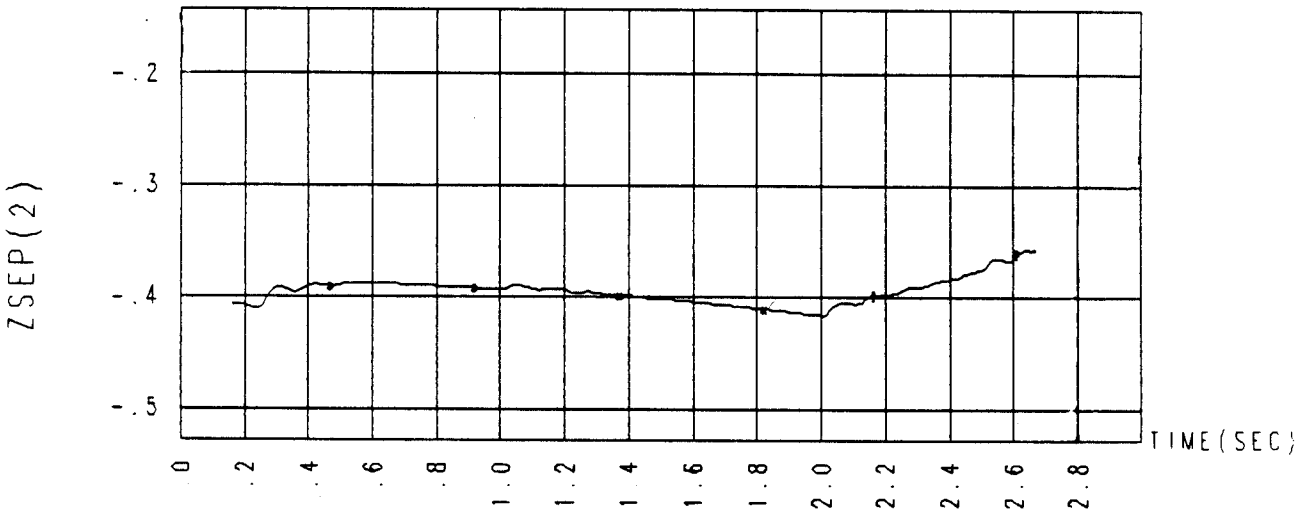

Figure 14

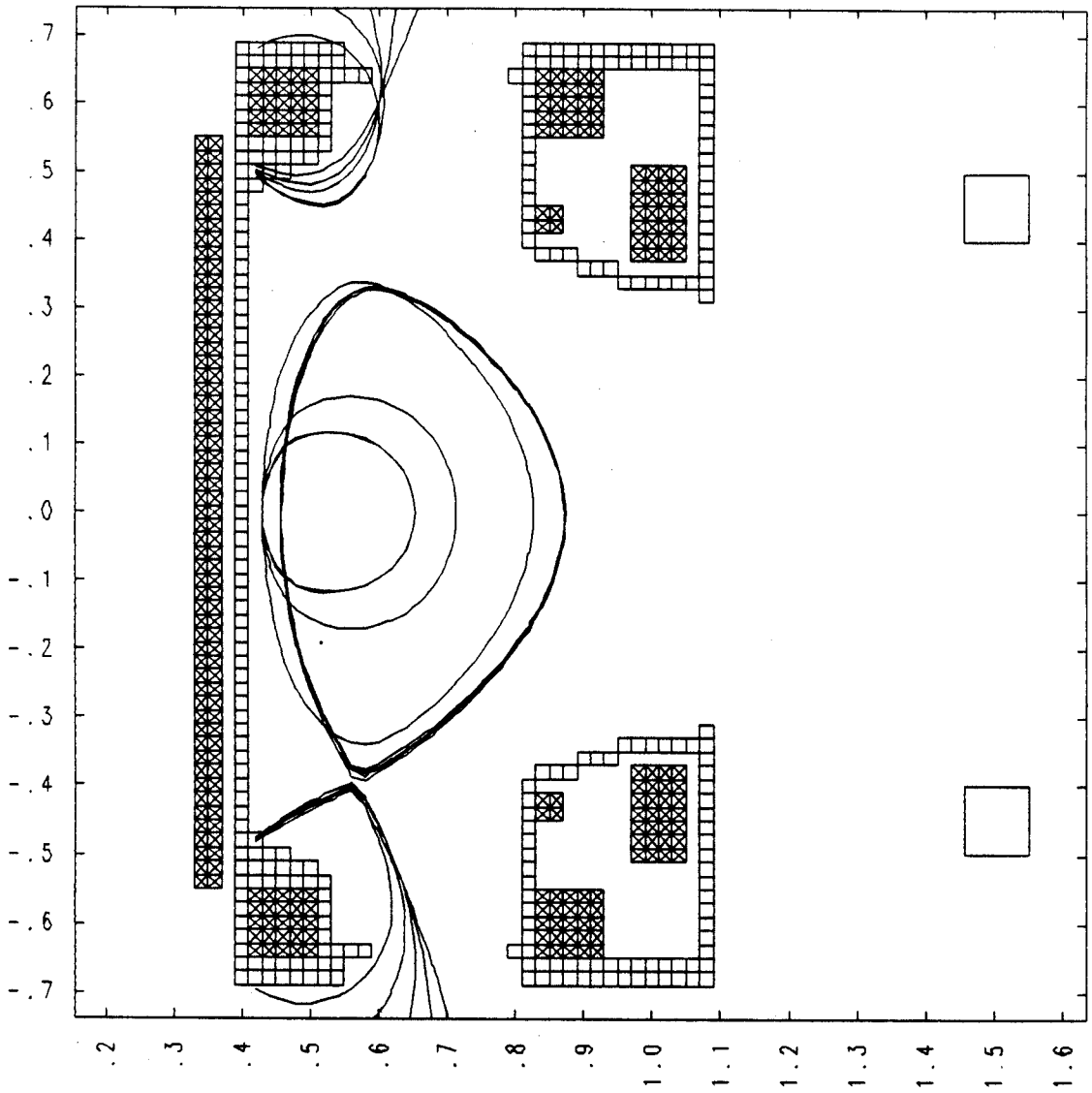

Figure 15

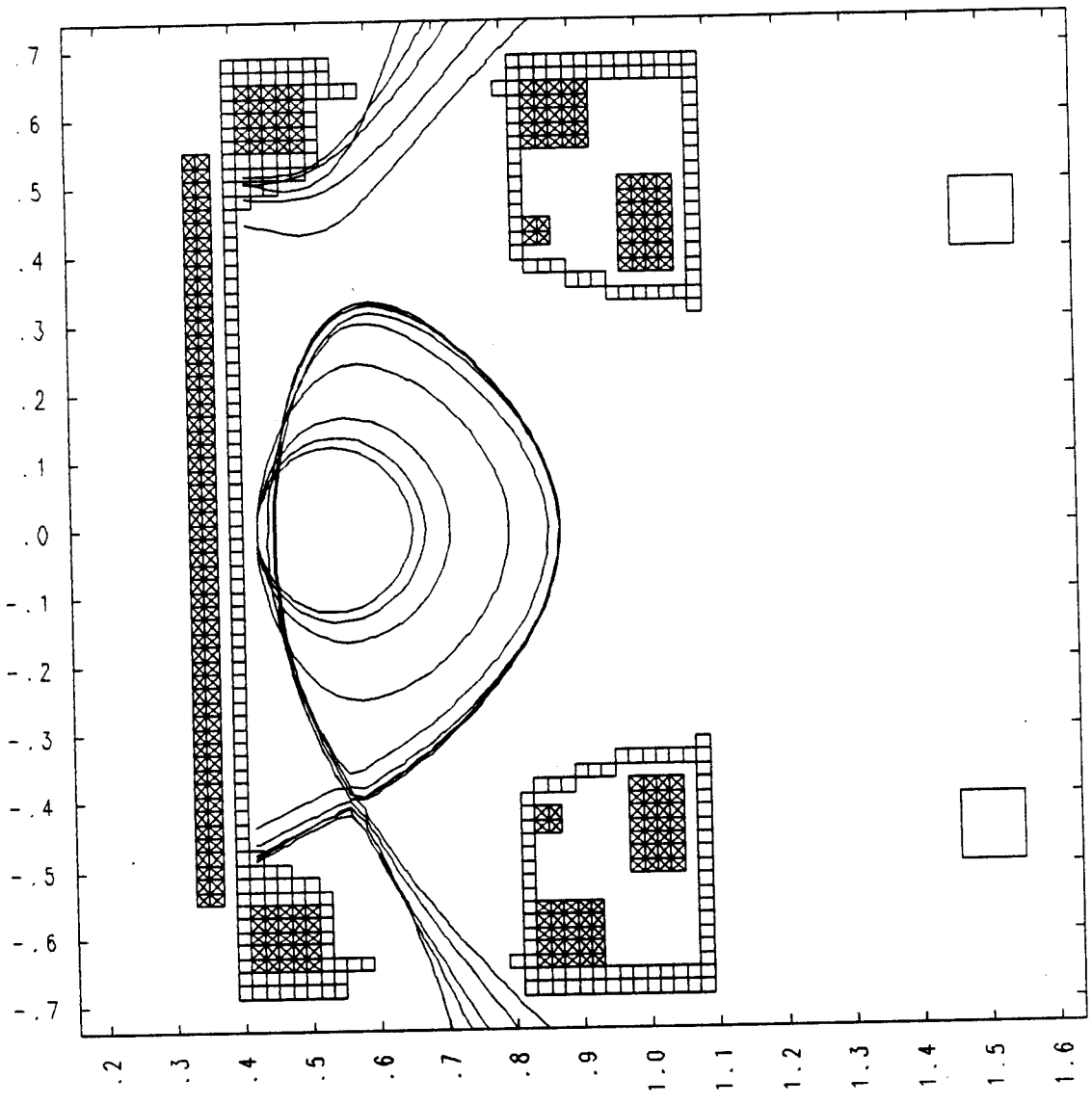

Figure 16

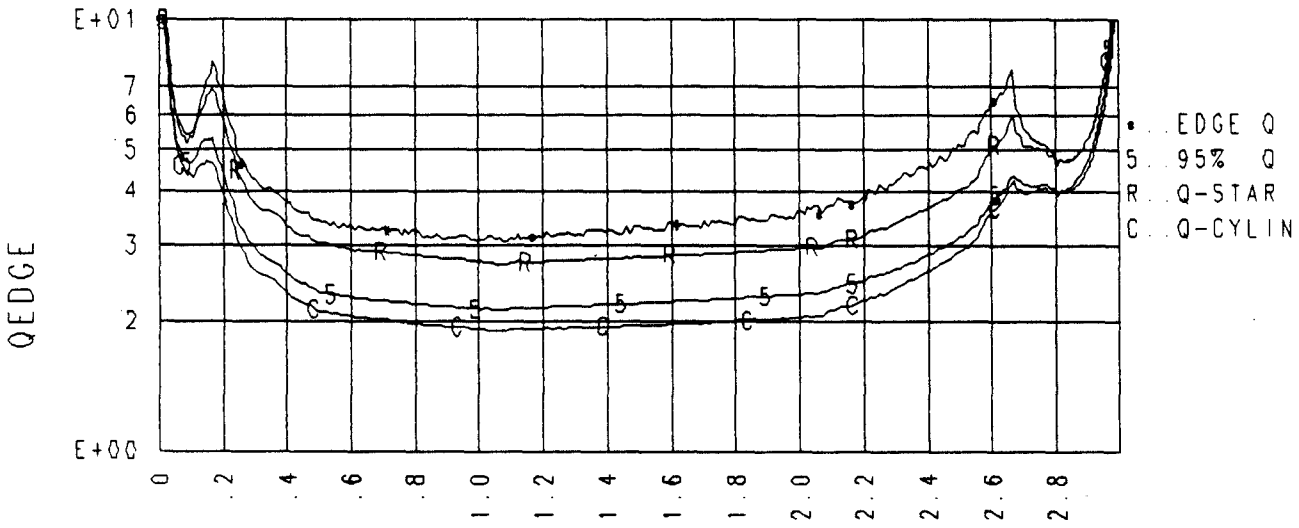
QEDGE
E+01
7
6
5
4
3
2
E+00
0
.2
.4
.6
.8
1.0
1.2
1.4
1.6
1.8
2.0
2.2
2.4
2.6
2.8
. EDGE Q
5 95% Q
R Q-STAR
C Q-CYLIN

Figure 17

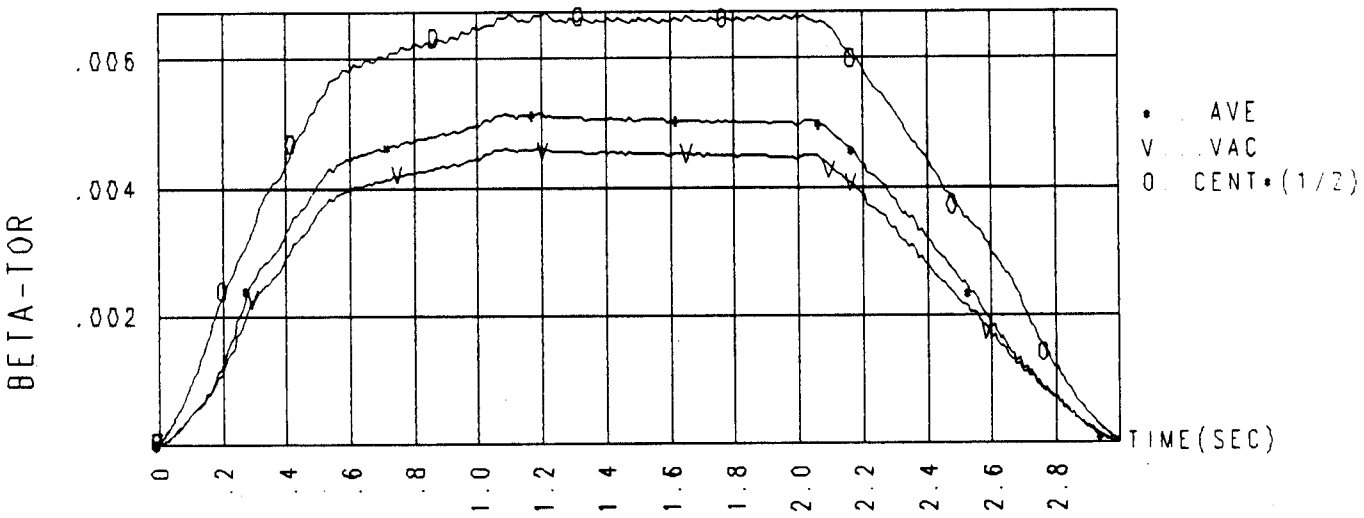
BETA-TOR
.006
.004
.002
0
.2
.4
.6
.8
1.0
1.2
1.4
1.6
1.8
2.0
2.2
2.4
2.6
2.8
TIME(SEC)
• AVE
V VAC
0 CENT•(1/2)

Figure 18

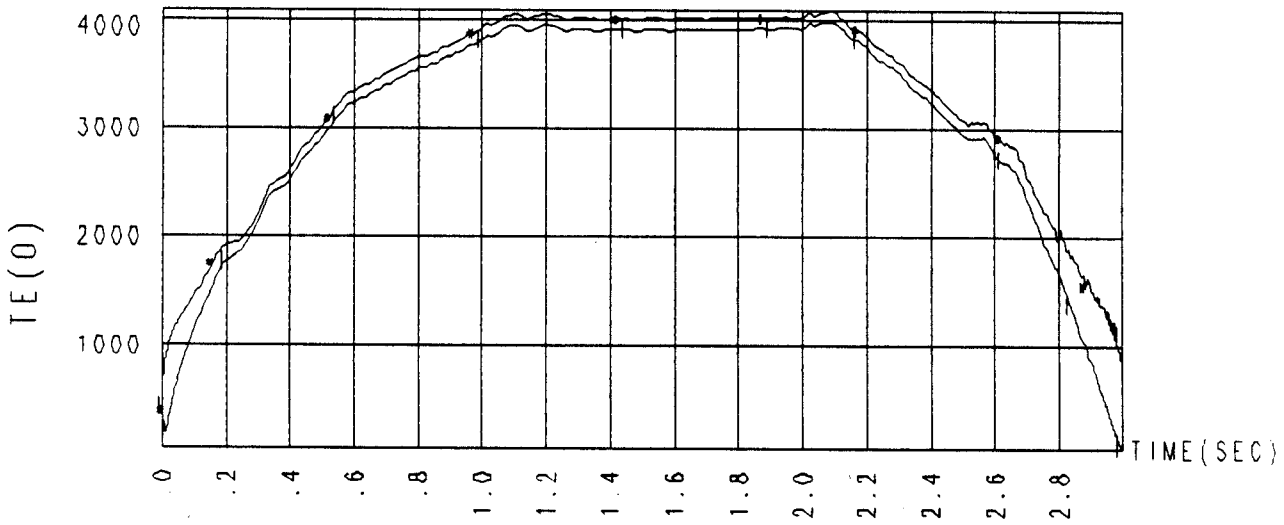
4000
3000
2000
1000
TE(0)
0
.2
.4
.6
.8
1.0
1.2
1.4
1.6
1.8
2.0
2.2
2.4
2.6
2.8
TIME(SEC)

Figure 19

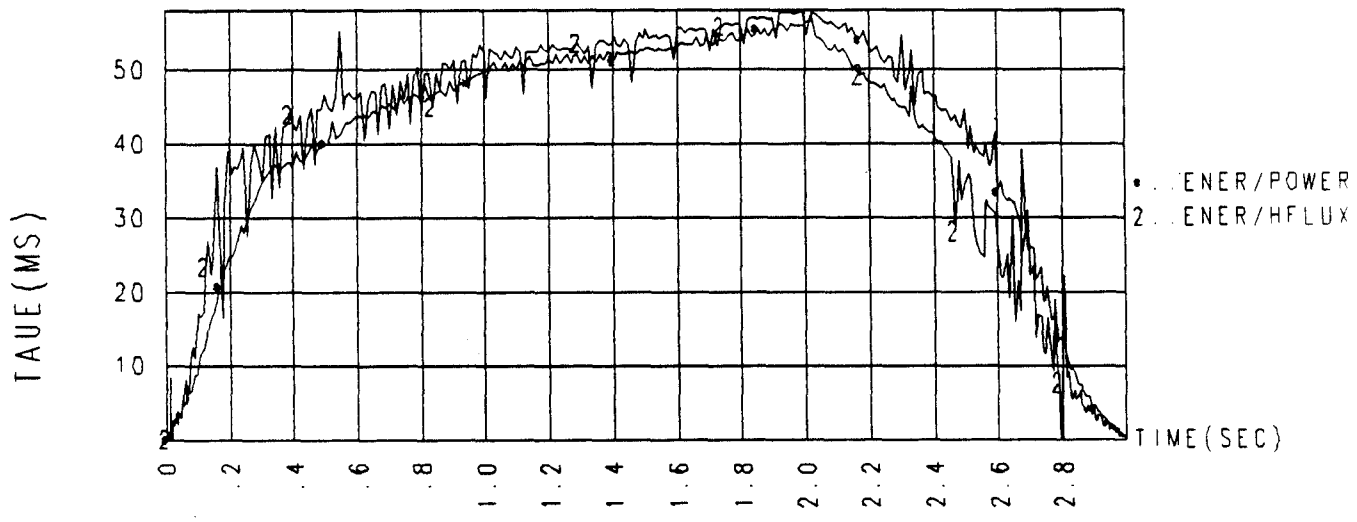
TAUE(MS)
50
40
30
20
10
0
.2
.4
.6
.8
1.0
1.2
1.4
1.6
1.8
2.0
2.2
2.4
2.6
2.8
TIME(SEC)
1 ENER/POWER
2 ENER/HFLUX

Figure 20

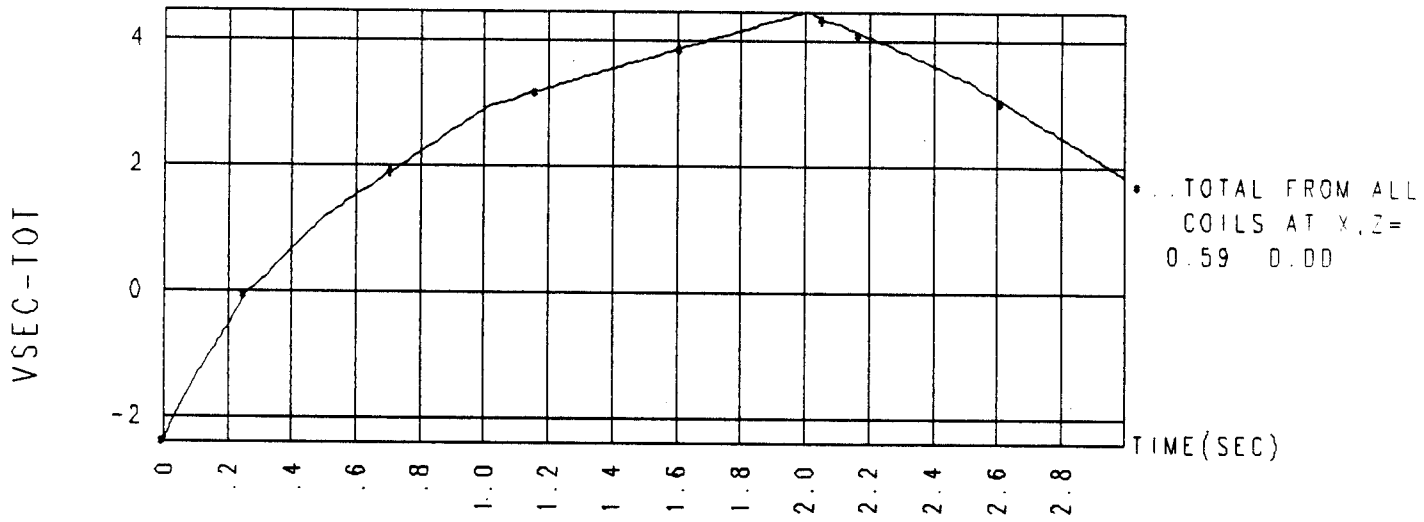
VSEC-TOT
4
2
0
-2
0
.2
.4
.6
.8
1.0
1.2
1.4
1.6
1.8
2.0
2.2
2.4
2.6
2.8
TIME(SEC)
TOTAL FROM ALL
COILS AT X,Z=
0.59 0.00

Figure 21

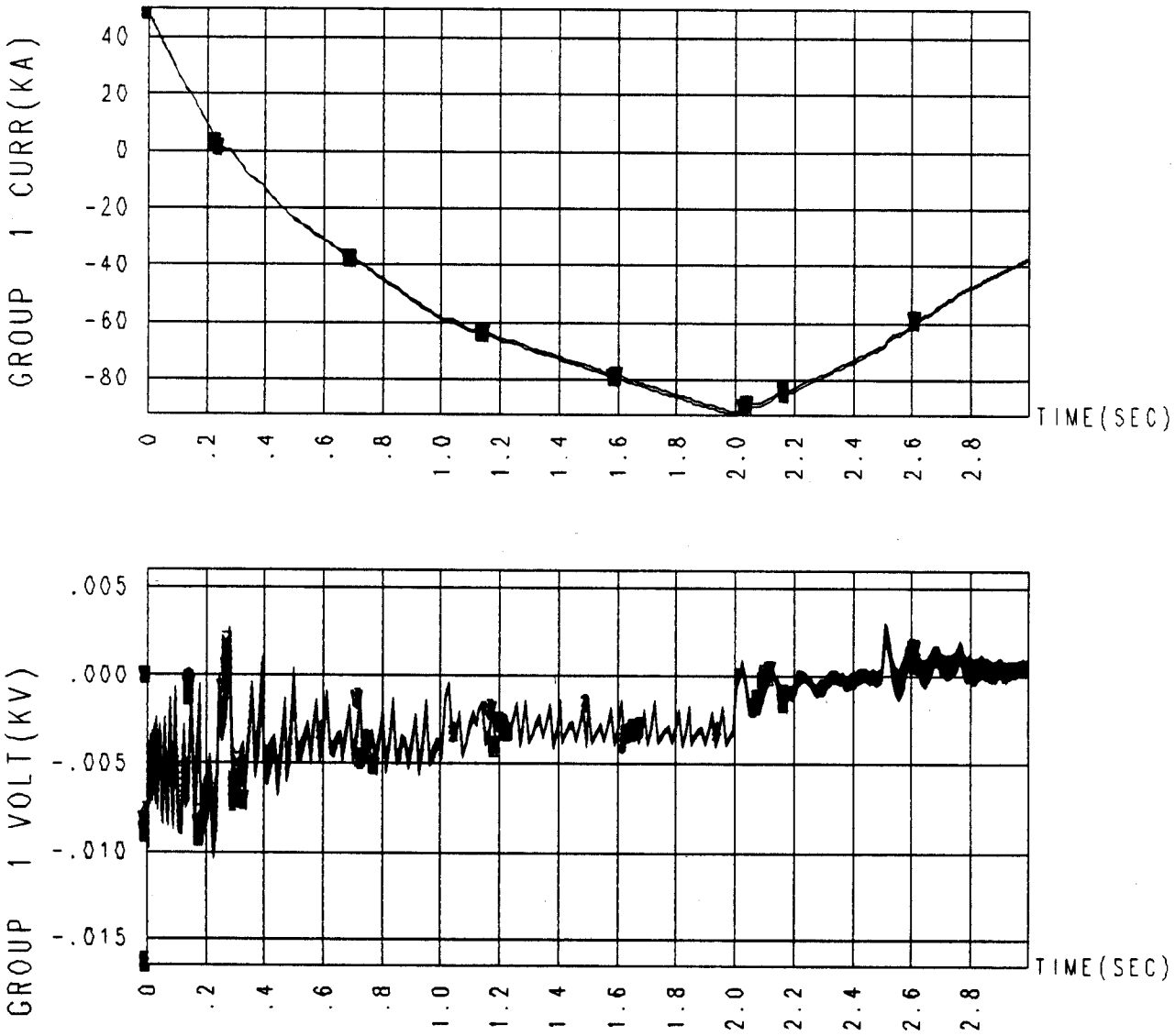
GROUP 1 CURR(KA)
40
20
0
-20
-40
-60
-80
0
.2
.4
.6
.8
1.0
1.2
1.4
1.6
1.8
2.0
2.2
2.4
2.6
2.8
TIME(SEC)
GROUP 1 VOLT(KV)
.005
.000
-.005
-.010
-.015
0
.2
.4
.6
.8
1.0
1.2
1.4
1.6
1.8
2.0
2.2
2.4
2.6
2.8
TIME(SEC)

Figure 22

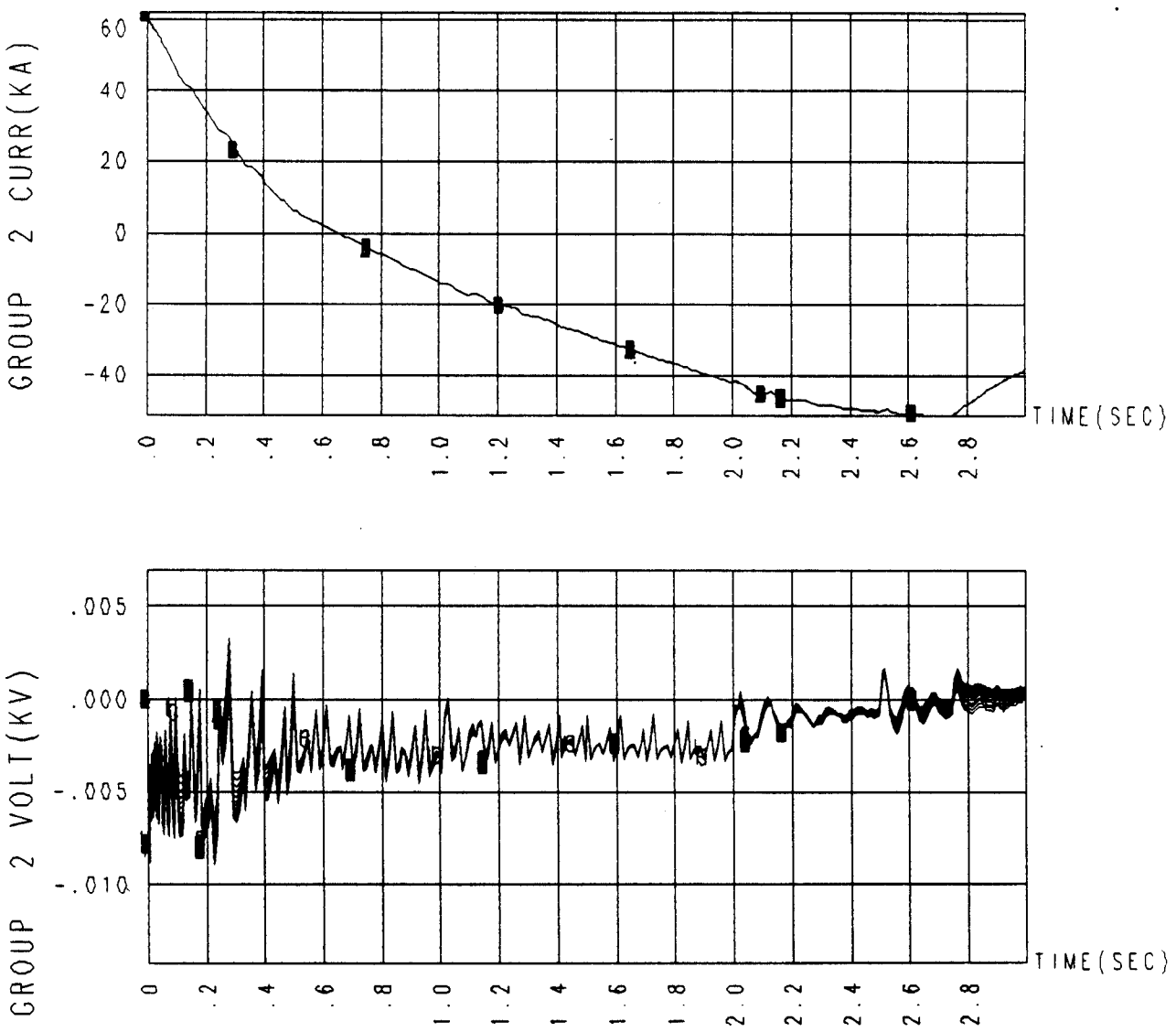
GROUP 2 CURR(KA)
60
40
20
0
-20
-40
0
.2
.4
.6
.8
1.0
1.2
1.4
1.6
1.8
2.0
2.2
2.4
2.6
2.8
TIME(SEC)
GROUP 2 VOLT(KV)
.005
.000
-.005
-.010
0
.2
.4
.6
.8
1.0
1.2
1.4
1.6
1.8
2.0
2.2
2.4
2.6
2.8
TIME(SEC)

Figure 23

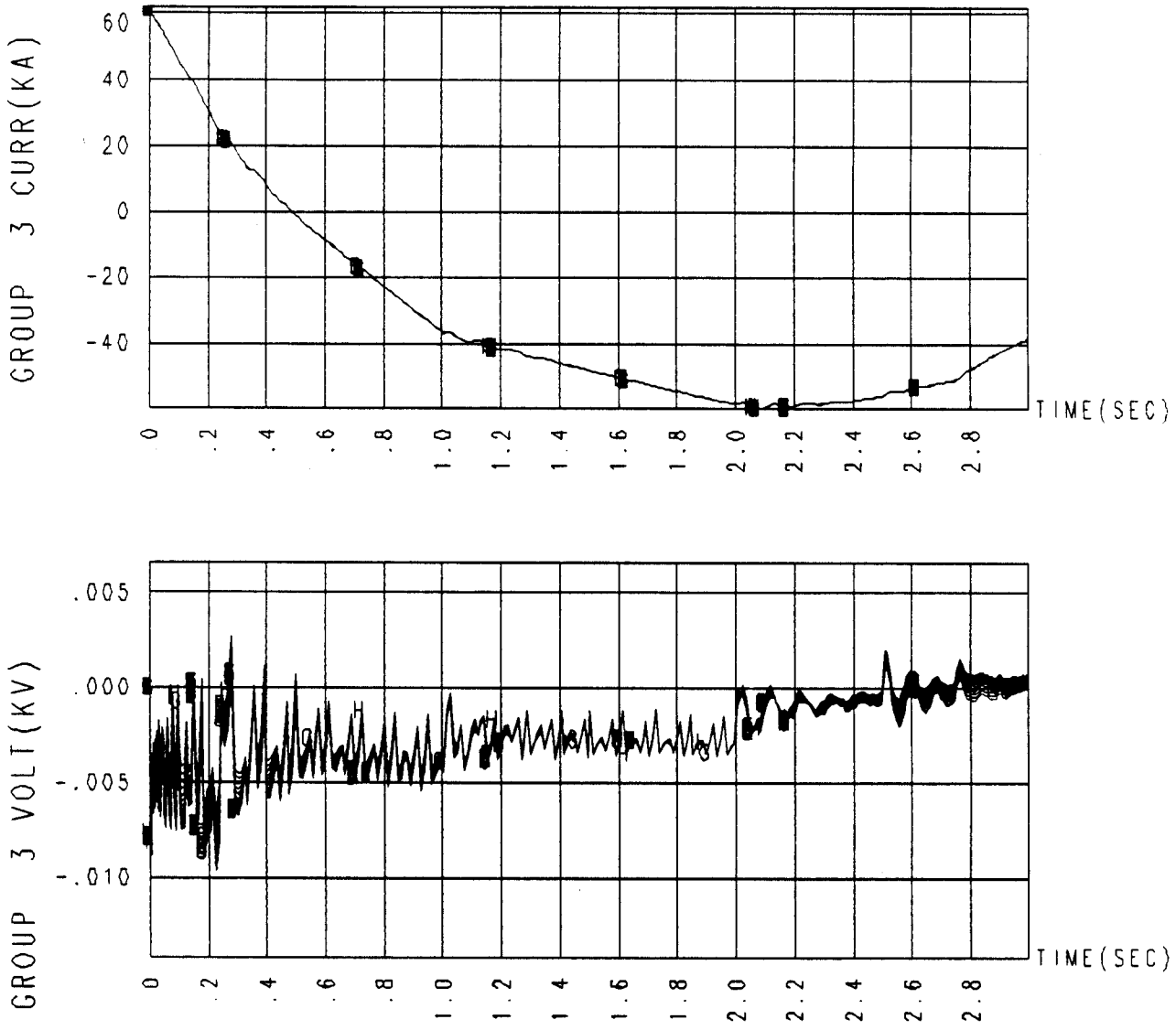
GROUP 3 CURR(KA)
60
40
20
0
-20
-40
0
.2
.4
.6
.8
1.0
1.2
1.4
1.6
1.8
2.0
2.2
2.4
2.6
2.8
TIME(SEC)
GROUP 3 VOLT(KV)
.005
.000
-.005
-.010
0
.2
.4
.6
.8
1.0
1.2
1.4
1.6
1.8
2.0
2.2
2.4
2.6
2.8
TIME(SEC)

Figure 24

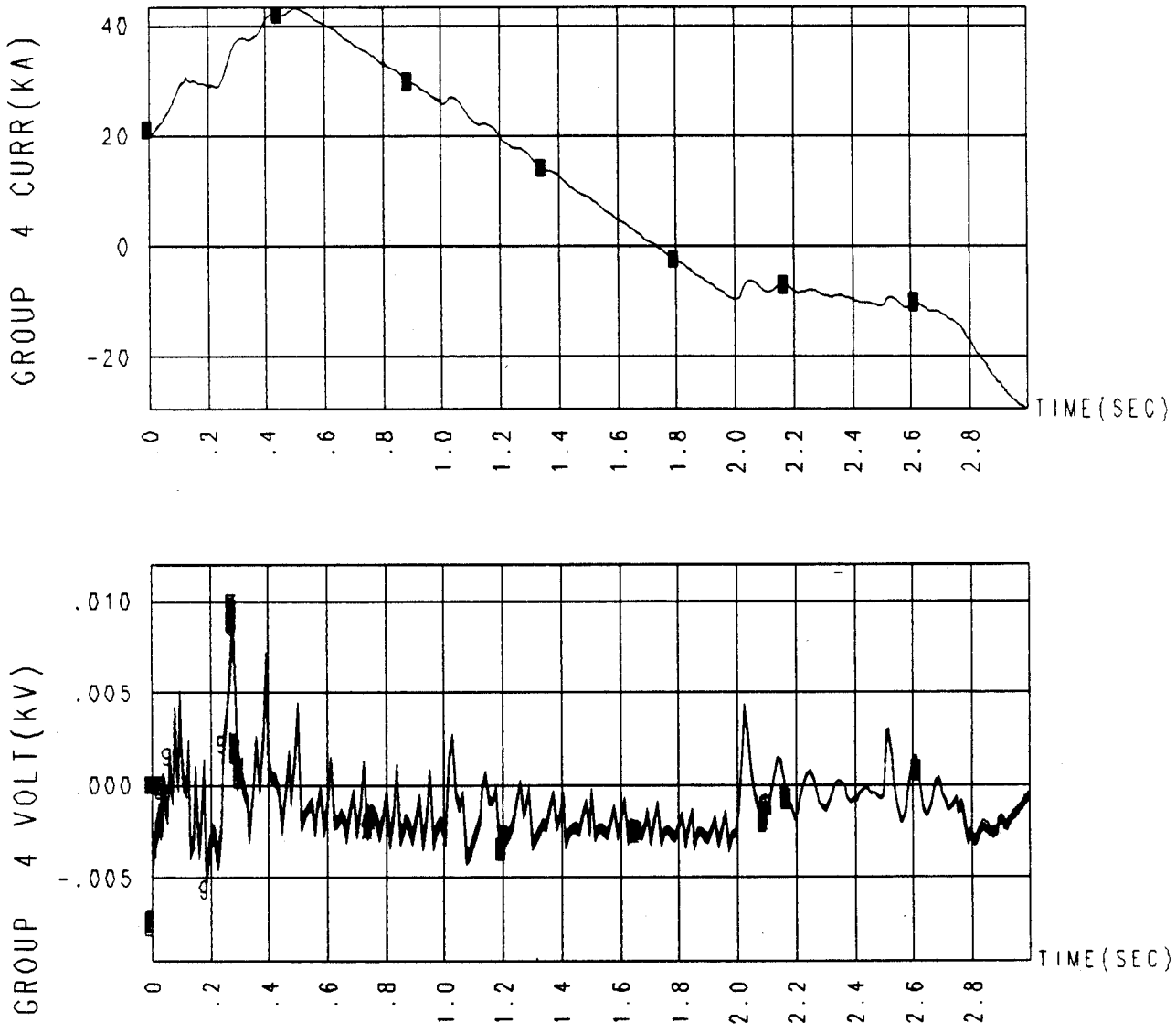
GROUP 4 CURR(KA)
40
20
0
-20
0
.2
.4
.6
.8
1.0
1.2
1.4
1.6
1.8
2.0
2.2
2.4
2.6
2.8
TIME(SEC)
GROUP 4 VOLT(KV)
.010
.005
.000
-.005
0
.2
.4
.6
.8
1.0
1.2
1.4
1.6
1.8
2.0
2.2
2.4
2.6
2.8
TIME(SEC)

Figure 25

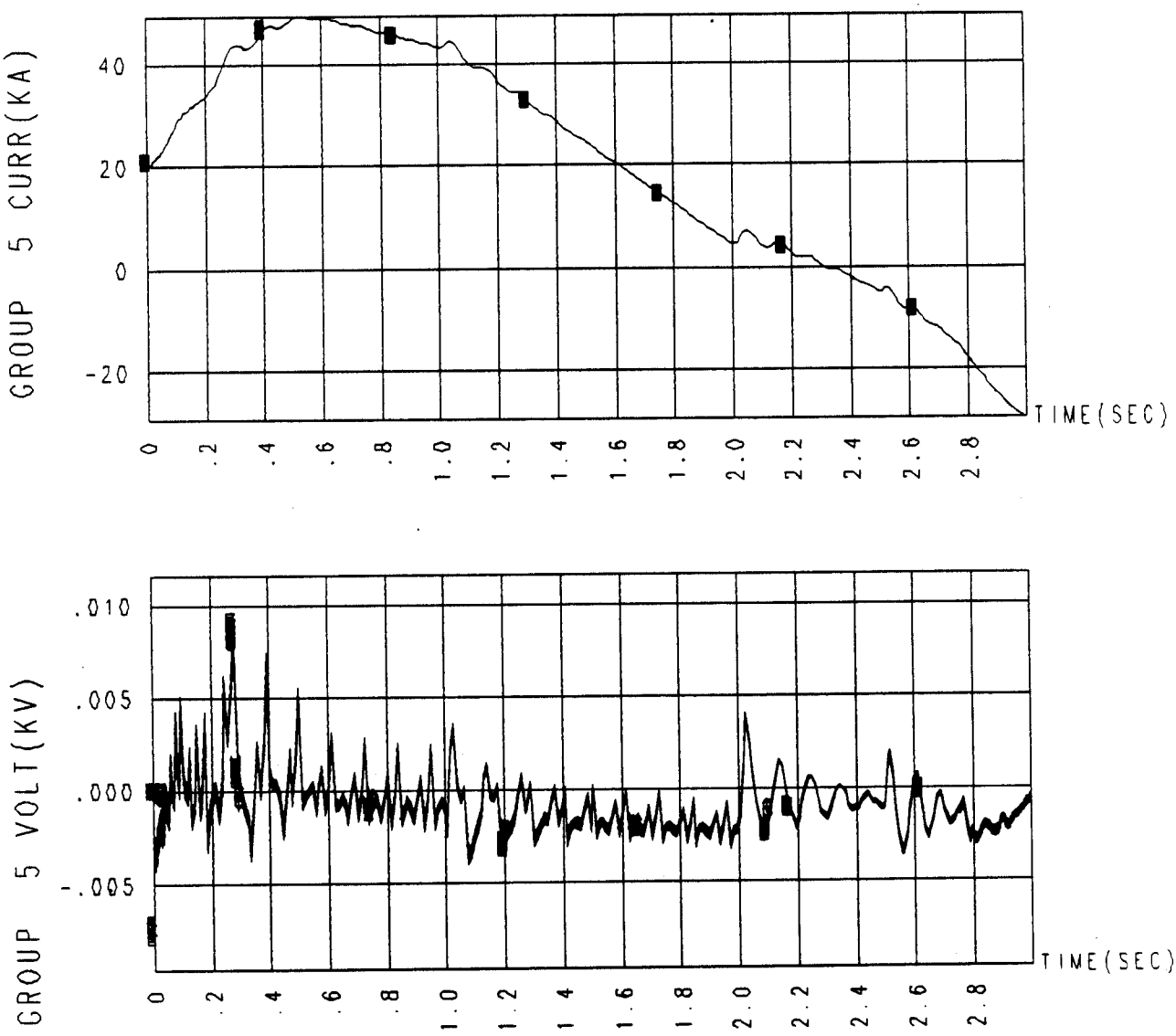
GROUP 5 CURR(KA)
40
20
0
-20
0
.2
.4
.6
.8
1.0
1.2
1.4
1.6
1.8
2.0
2.2
2.4
2.6
2.8
TIME(SEC)
GROUP 5 VOLT(KV)
.010
.005
.000
-.005
0
.2
.4
.6
.8
1.0
1.2
1.4
1.6
1.8
2.0
2.2
2.4
2.6
2.8
TIME(SEC)

Figure 26

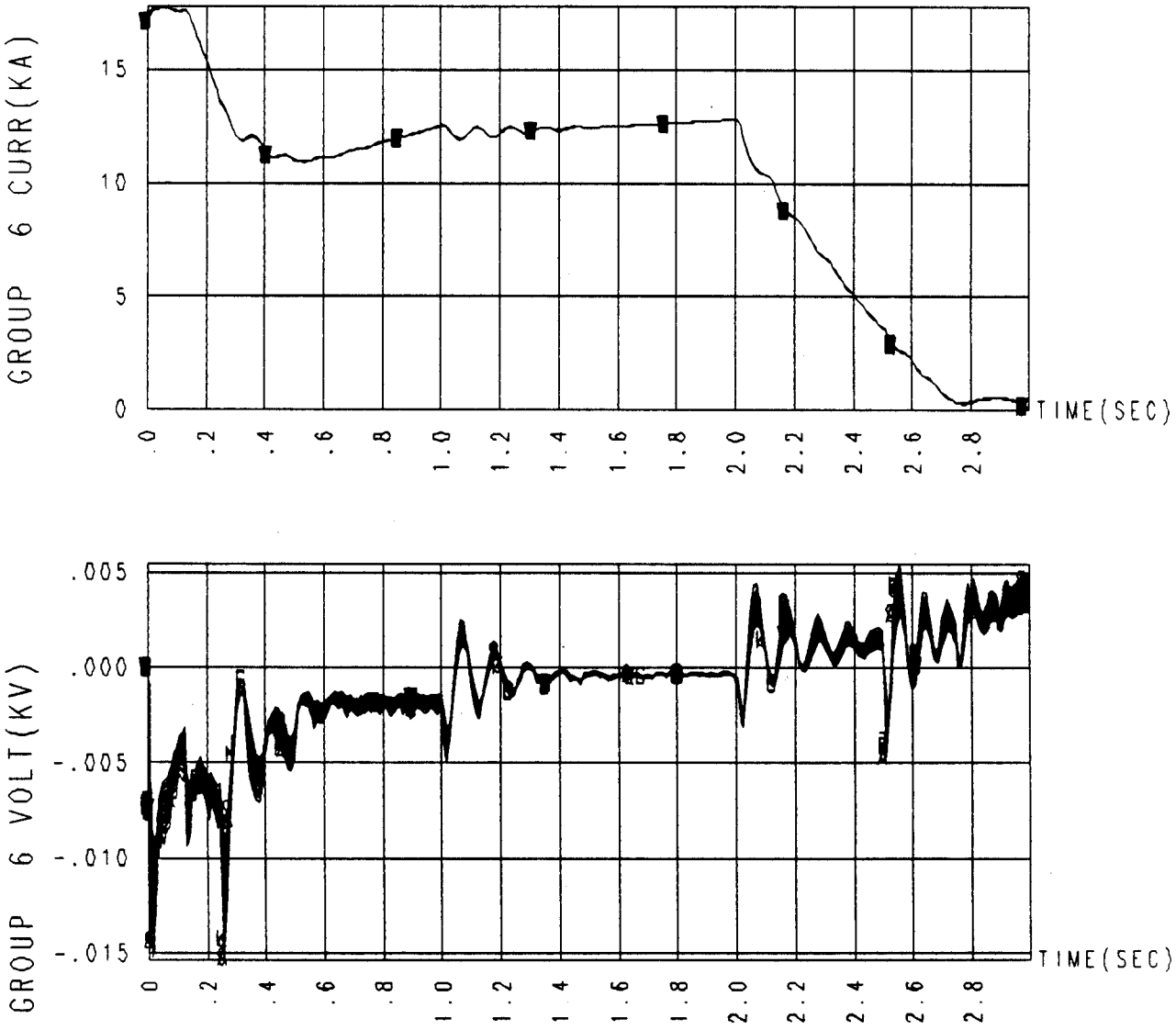
GROUP 6 CURR(KA)
15
10
5
0
.0
.2
.4
.6
.8
1.0
1.2
1.4
1.6
1.8
2.0
2.2
2.4
2.6
2.8
TIME(SEC)
GROUP 6 VOLT(KV)
.005
.000
-.005
-.010
-.015
0
.2
.4
.6
.8
1.0
1.2
1.4
1.6
1.8
2.0
2.2
2.4
2.6
2.8
TIME(SEC)

Figure 27

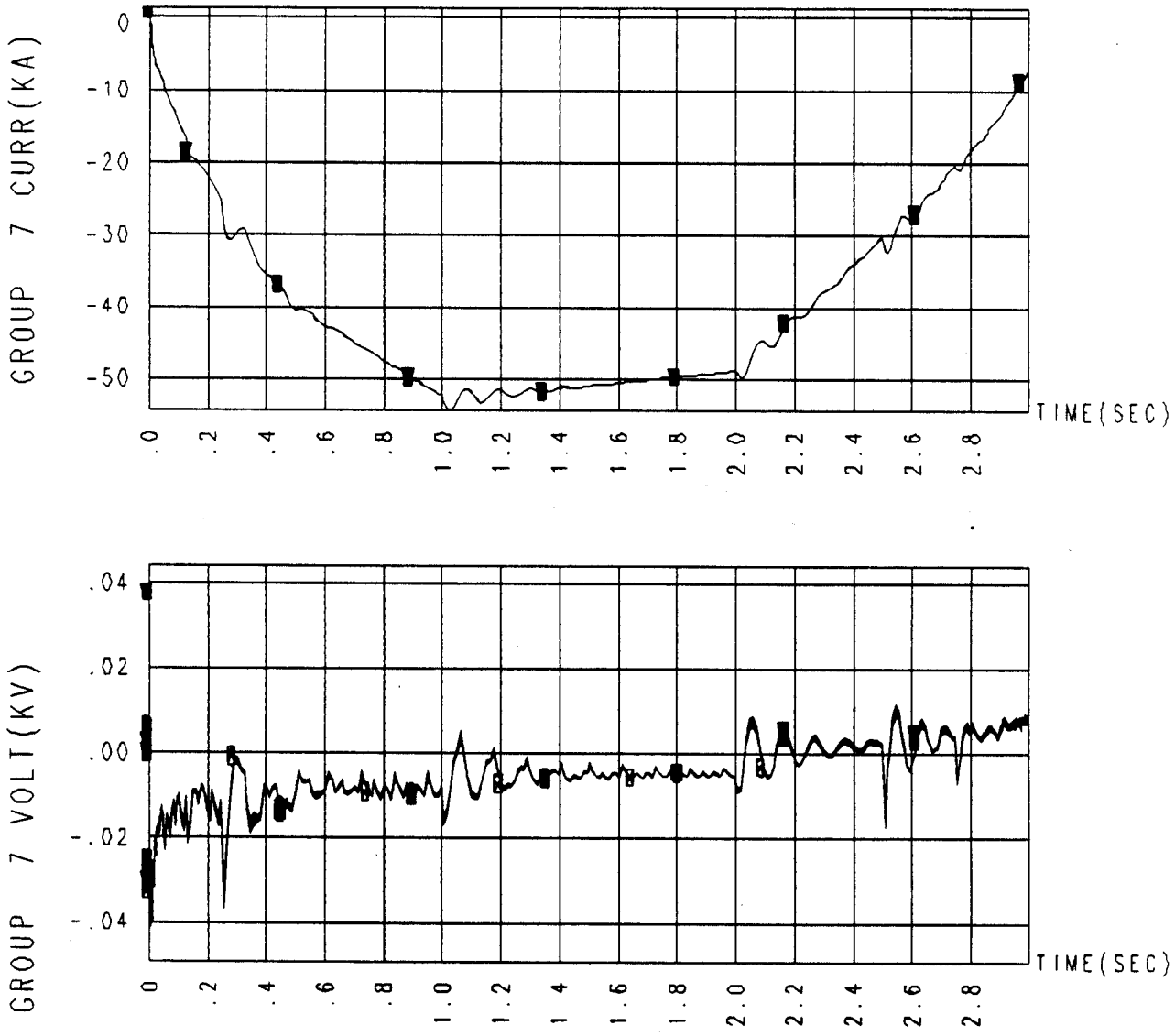
GROUP 7 CURR(KA)
0
-10
-20
-30
-40
-50
TIME(SEC)
0
.2
.4
.6
.8
1.0
1.2
1.4
1.6
1.8
2.0
2.2
2.4
2.6
2.8
GROUP 7 VOLT(KV)
.04
.02
.00
-.02
-.04
TIME(SEC)

Figure 28

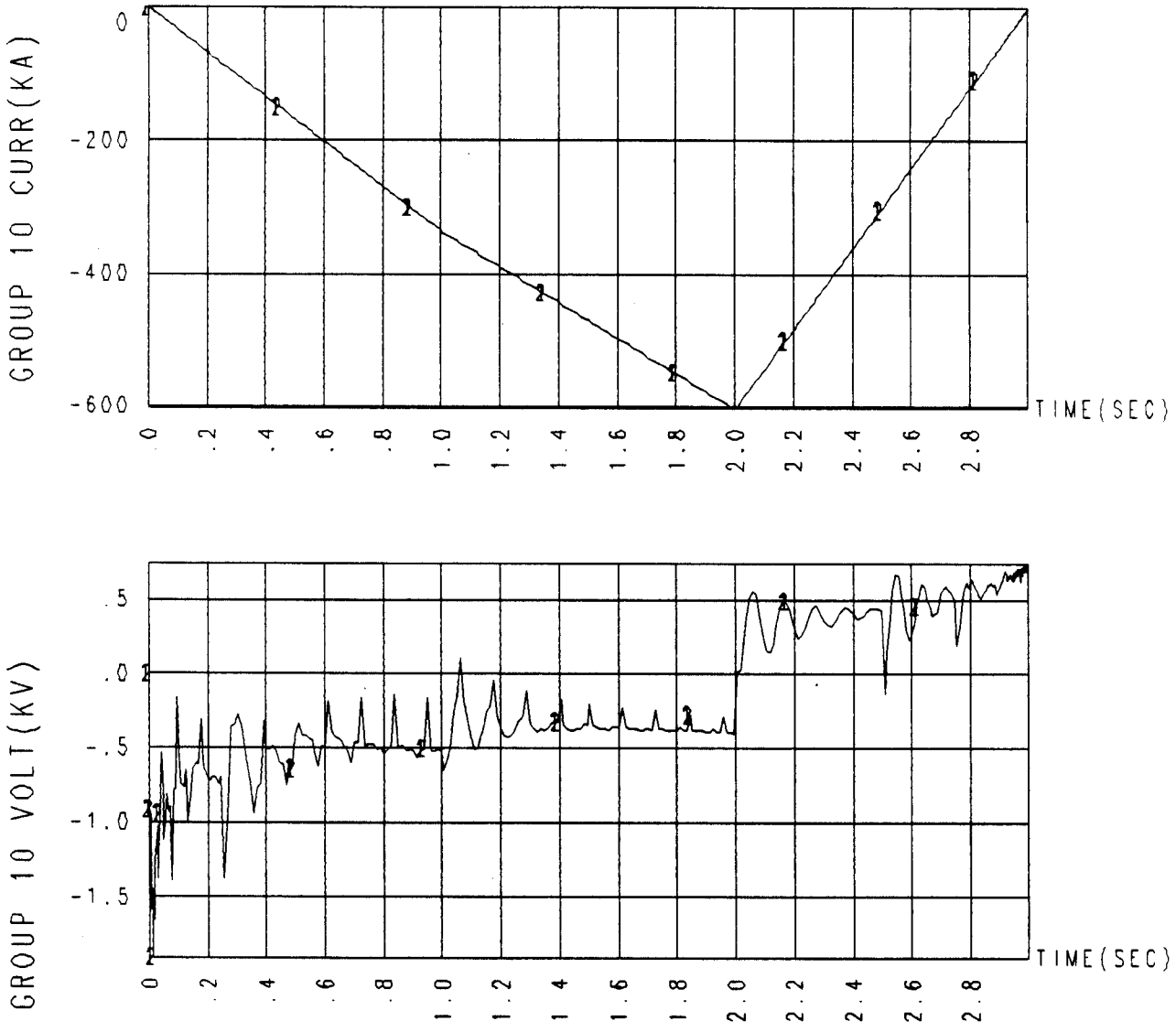
GROUP 10 CURR(KA)
0
-200
-400
-600
0
.2
.4
.6
.8
1.0
1.2
1.4
1.6
1.8
2.0
2.2
2.4
2.6
2.8
TIME(SEC)
GROUP 10 VOLT(KV)
.5
.0
-.5
-1.0
-1.5
0
.2
.4
.6
.8
1.0
1.2
1.4
1.6
1.8
2.0
2.2
2.4
2.6
2.8
TIME(SEC)

Figure 29

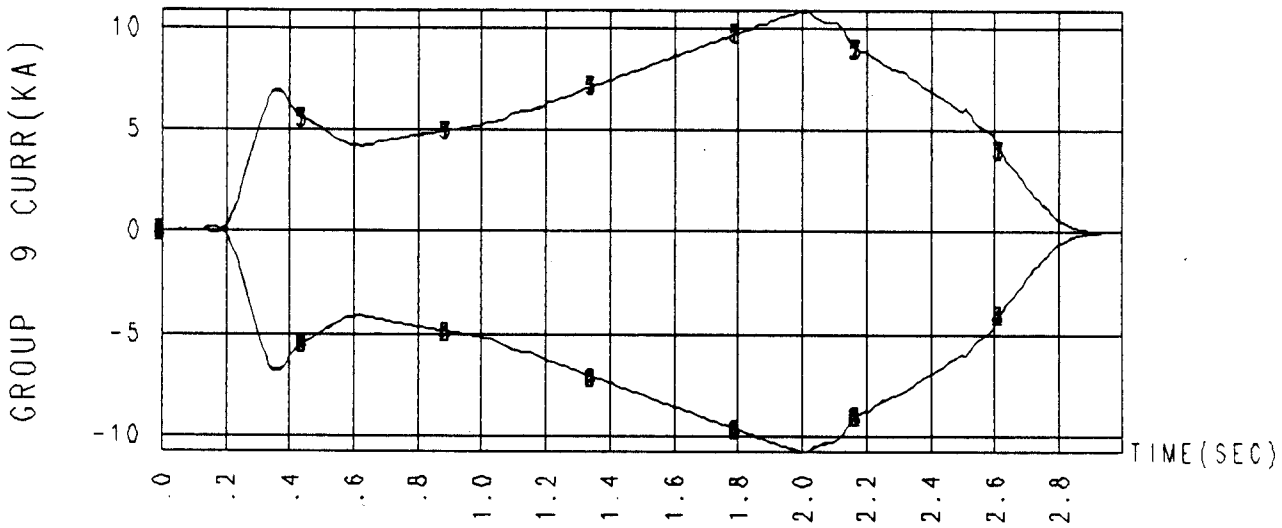
GROUP 9 CURR(KA)
10
5
0
-5
-10
0
.2
.4
.6
.8
1.0
1.2
1.4
1.6
1.8
2.0
2.2
2.4
2.6
2.8
TIME(SEC)

Figure 30

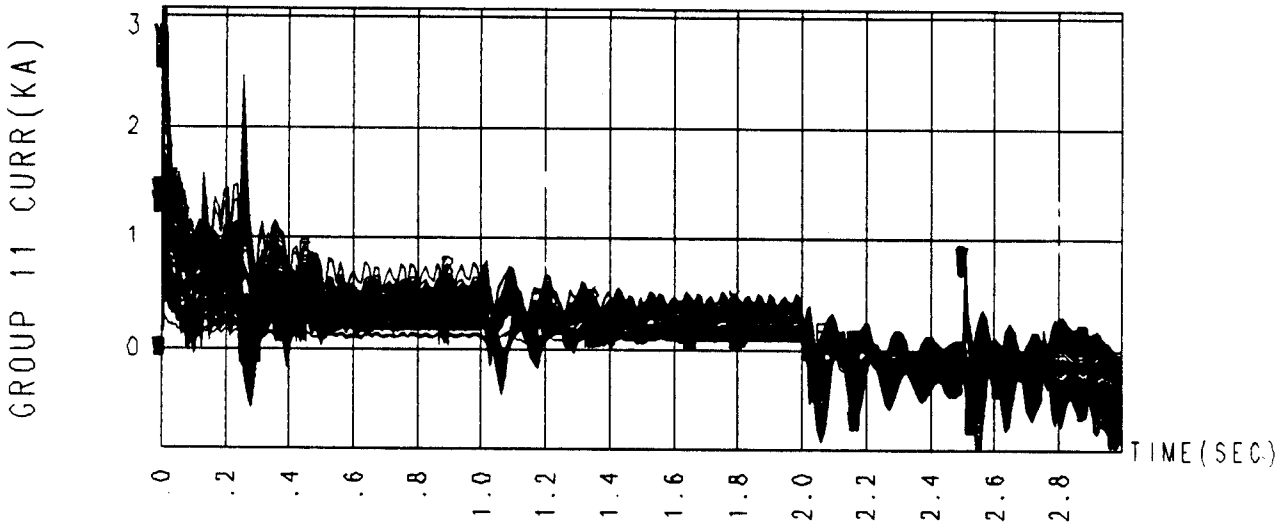

Figure 31